Journal of Applied Polymer Science

Spatially Resolved Monitoring of Crystalline Suprastructure and Molecular Orientation in α- and β-Nucleated Polypropylene Pipes Using Differential Scanning Calorimetry, Infrared Microscopy, and Polarized Light Microscopy

Tobias Schuster,[1] Karsten Rode,[1] Robert Brüll,[1] Jürgen Heinemann,[2] Hansgeorg Haupt[2]

[1]Division Plastics, Fraunhofer LBF, 64289 Darmstadt, Germany

[2]Technische Universität Darmstadt, Zentrum für Konstruktionswerkstoffe (MPA, IfW), 64283 Darmstadt, Germany

Correspondence to: R. Brüll (E-mail: robert.bruell@lbf.fraunhofer.de).

ABSTRACT: Differently nucleated polypropylene (PP) pipes were studied by polarized light and infrared (IR) microscopy and differential scanning calorimetry (DSC). Although Fourier transform IR microscopy (μFTIR) excels by high spatial resolution and ease of measurement over the classical approach with manually prepared sections and individual analysis, a disadvantage is that the vibrational bands used to calculate the degree of crystallinity may be influenced by the polymorphism of PP. While this does not play a role for the α-polymorph, in the case of β-nucleated PP the calculated profile of crystallinity derived from the so called crystallinity bands depends on the direction of inspection. We could show that in the case of β-nucleation the results from μFTIR and DSC of cross-sections can be correlated, and thus the crystallinity profile obtained from μFTIR becomes independent from the direction of consideration. Consequently the advantages of μFTIR with regard to spatial resolution and reproducibility can now be exploited for β-nucleated PP as well. Using the differently nucleated specimen we give the first practical validation of a previously on a theoretical basis derived model to determine the molecular orientation in all three dimensions (machine, transverse, and normal). It could be shown that the profiles of molecular orientation are a function of both, the extrusion process with its post extrusion cooling conditions, and the type of nucleating agent. © 2013 Wiley Periodicals, Inc. J. Appl. Polym. Sci. 130: 4182–4190, 2013

KEYWORDS: crystallization; differential scanning calorimetry; microscopy; spectroscopy; polyolefins

Received 26 February 2013; accepted 23 June 2013; Published online 13 July 2013

DOI: 10.1002/app.39704

INTRODUCTION

A considerable percentage of the total conception of pipes in household and industrial usage is undertaken by polyolefins because of their advantageous properties, and this is one of the main reasons for the increased attention toward research in polyolefin pipes. They are commonly produced by extrusion, during which the molten resin is pressed through a die and the semifinished product enters a so called calibration line. Within the latter step, the hot pipe is cooled from the outside with water, while the lumen is filled with hot air. When passing the water bath, the molten polymer solidifies and the morphology of the pipe wall is formed. As a result of the thermal conditions a gradient of temperature exists after entering the water bath, i.e., quenching occurs at the outer pipe wall where the melt is exposed to water, whereas the inner sections gradually crystallize.[1] The resulting morphology, i.e., the degree of crystallinity, type and quantity of polymorphs and the crystallite size distribution can be controlled by nucleating agents.[2–12] Among the polyolefins polypropylene (PP) has an extremely versatile crystallization behavior due to its polymorphism.[13–15]

On the analytical side the degree of crystallinity, i.e., the ratio of crystalline to amorphous phase, the alignment of the polymer chains, i.e., their orientation, and the distribution of the spherulite size are the fundamental parameters. However, as the cooling conditions within the pipe wall may vary within a wide range, the morphological parameters will vary accordingly. Polarized light microscopy (PLM) is widely used to analyze the morphological structure with regard to type and size of spherulites.[12,14,16–21] Particularly, the "core–shell" structure formed in polymer pipes can be studied.[1,22]

On the contrary Fourier transform IR microscopy (μFTIR) excels by offering quantitative information with regard to composition.[23,24] It has also been widely used to study morphological features like orientation of polymer chains and degree of crystallinity.[25–28] However, when interpreting the data it has to

be taken into account that these parameters are not independent from each other. So far differential scanning calorimetry (DSC) has been used to determine the degree of crystallinity and polymorphism.[18,29,30] Spatial resolution can be achieved by controlled mechanical abrasion samples and analyzing them individually. In this study we want to investigate two differently nucleated PP pipes with regard to their crystalline suprastructure, i.e., spherulite size, polymorphism, and degree of crystallinity. In particular we want to show how μFTIR can be used to determine the degree of crystallinity and molecular orientation in both α- and β-nucleated PP and thus exploit the benefits of this technique with regard to ease of measurement and spatial resolution.

EXPERIMENTAL

Material

Pipes produced from isotactic PP (homopolymer, i-PP-H) with a wall thickness of 5.8 mm and an outer diameter of 63 mm were obtained directly from the manufacturers. Two kinds of i-PP-H were used: One α-nucleated and one β-nucleated, termed as PP1 and PP2, respectively. The nucleating agent used were 500 ppm methylene-bis(4,6-di-tert-butylphenyl) phosphate sodium salt for PP1 and 500 ppm pimelic acid, calcium salt for PP2. Both have broad molar mass distributions, as measured by gel permeation chromatography (see Table I).

Polarized Light Microscopy

A microscope (BX50 F, Olympus) equipped with UPlan objectives, a rotatable polarizer (U-POT), analyzer (U-AN360) and a compensator plate (U-TP530) was used. 12 V lamp and 35 ms illumination time was set for imaging. The software was analySIS auto 5.1. A resin was used to fix the microtomed sections onto glass slides. Microtome cuts of 10 μm thickness parallel (cut_{II}) and perpendicular ($cut_{\perp}$) to the direction of extrusion were analyzed.

Differential Scanning Calorimetry

Circular samples with a diameter of 5 mm and a thickness of 300 μm (ca. 5 mg) were peeled from the outer surface of the pipe and were analyzed with a Mettler Toledo DSC 822e. For an accurate measurement the instrument was calibrated with high purity indium and zinc standards. All samples were measured with a heating rate of 10°C/min under an inert atmosphere of nitrogen between 25 and 230°C and the first heating cycle was used to calculate the degree of crystallinity (X_C^{DSC}) and the ratio of α- to β-polymorph.

$\Delta H^0_\alpha = 177\,\frac{J}{g}$ and $\Delta H^0_\beta = 168\,\frac{J}{g}$ were chosen for the heat of fusion for the completely crystalline α- and β-modification, respectively.[31] The fractional percentages of the total X_C^{DSC} of the α- (K_α) and β-modification (K_β) were determined according to the following equation:

$$K_\alpha = \frac{\frac{\Delta H_\alpha}{\Delta H^0_\alpha}}{\left(\frac{\Delta H_\beta}{\Delta H^0_\beta} + \frac{\Delta H_\alpha}{\Delta H^0_\alpha}\right)} \quad (1)$$

$$K_\beta = \frac{\frac{\Delta H_\beta}{\Delta H^0_\beta}}{\left(\frac{\Delta H_\beta}{\Delta H^0_\beta} + \frac{\Delta H_\alpha}{\Delta H^0_\alpha}\right)} \quad (2)$$

ΔH_α and ΔH_β are the enthalpy of fusion of the α and β form in samples with mixed polymorphic composition and can be determined by the area of the melting peaks (Figure 1).[32] The entire enthalpy of fusion (ΔH^0) was calculated with the following equation:

$$\Delta H^0 = K_\alpha \cdot \Delta H^0_\alpha + K_\beta \cdot \Delta H^0_\beta \quad (3)$$

The ratio of the actual enthalpy (ΔH), which is the sum of ΔH_α and ΔH_β, and ΔH^0 represents X_C^{DSC} as indicated in the following equation:

$$X_C^{DSC} = \frac{\Delta H}{\Delta H^0} \cdot 100 \quad (4)$$

IR Microscopy

Cuts of 100 μm thickness were microtomed perpendicular ($cut_{\perp}$) and parallel (cut_{II}) to the extrusion direction. An infrared microscope (Continuum, Thermo Nicolet (Madison, WI) equipped with a MCT-A-detector was used for analysis. It was coupled to a Nicolet-Nexus 670 FTIR spectrometer as beam source. 100 scans were accumulated per spectrum using an aperture of 100 μm × 100 μm. The step width of the line scans was 100 μm. A microvice sample holder was used to fix the sample. All measurements were carried out in transmission mode. The details of sample preparation have been described elsewhere.[28]

A ZnSe wire-grid polarizer was used for the dichroic measurements. For the angle α, between the transition moment vector of the dipole and the polymer chain axis, 18° was used (Table II).[33]

The orientation was measured using linear polarized light with an electric vector parallel to transversal (TD), normal (ND),

Table I. Type and Properties of Pipes

Sample	Compound	Nucleation	Average molar mass[a] (g/mol)	Melt flow index[b] (g/10min)	Density (g/cm^3)
PP1-D63	PP1	α	$\bar{M}_w = 5.7 \cdot 10^5$	0.30	0.915
			$\bar{M}_n = 1.6 \cdot 10^5$		
PP2-D63	PP2	β	$\bar{M}_w = 1.1 \cdot 10^6$	0.30	0.905
			$\bar{M}_n = 2.6 \cdot 10^5$		

[a] Calibrated versus polystyrene standards.
[b] Melt flow index at 230°C, 2.16 kg.

Applied Polymer SCIENCE

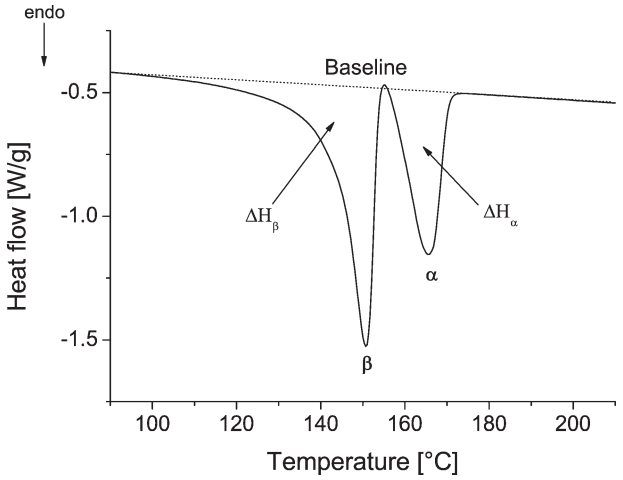

Figure 1. DSC melting curve of PP2-D63.

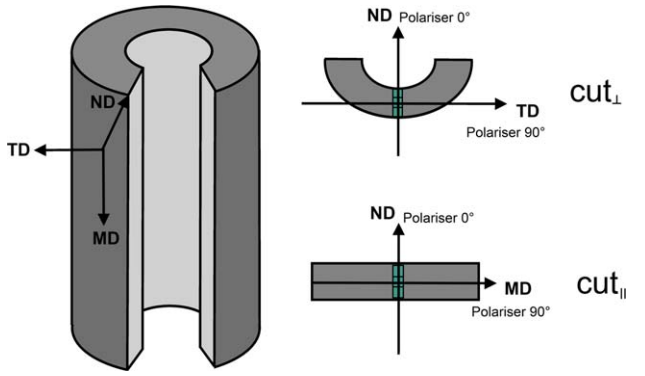

Figure 2. Indication of orientation in transversal (TD), normal (ND), and machine (MD) directions. [Color figure can be viewed in the online issue, which is available at wileyonlinelibrary.com.]

and machine (MD) directions, respectively (see Figure 2 for illustration).

RESULTS AND DISCUSSION

Processed polymers are spatially distributed with regard to their morphological parameters. To analyze these distributions independent from each other is a prerequisite to establish processing → property relationships. PLM is frequently used to study anisotropy in polymers. In PLM a microtome cut is placed between two linear polarizers aligned perpendicular to each other. This means that in the case of an isotropic sample no light will be transmitted to the detector, whereas in the case of an anisotropic sample the oscillating plane of the light is rotated and a certain portion of light may pass the second polarizer. Figure 3 presents PLM micrographs of PP1-D63 and PP2-D63 measured at identical illumination conditions.

PP1 and PP2 differ significantly in brightness. β spherulites are highly birefringent which causes the high brightness of the PP2 sample.[14] Comparing the images of the respective cutting directions shows clear differences in brightness and a gradient of the latter over each cut. For a more quantitative comparison the histograms are shown in Figure 4.

For PP1-D63 differences are only observed for the outer half of the pipe. The brightness in cut$_{\parallel}$ decreases almost linearly from inside to outside, whereas for cut$_{\perp}$ the profile is almost constant over the inner half of the pipe wall and decreases in the outer part. In the case of PP2-D63 differences in brightness between the cuts are observed over the entire pipe wall. It is noteworthy that a discontinuity in brightness exists at the wall center for cut$_{\perp}$ but not for cut$_{\parallel}$. Comparing the brightness of PP1-D63 and PP2-D63 reveals that for both materials the highest contrast between the two orthogonal cuts is visible in the outer part of the wall, and it may therefore be assumed that orientation induced by shear stress during production and subsequent freezing is the underlying reason.

A first order retardation plate which enables to determine the optical sign of birefringence was used to discriminate the polymorphs.[35] As a result type and size of the spherulites can be analyzed. In Figure 5, the section from the inner part of PP1-D63 and PP2-D63 taken at comparable positions is presented.

The two polymorphs can easily be distinguished: Negative optical birefringence causes the first and third quadrant of the spherulite to show a yellow color, whereas in the case of positive birefringence the second and fourth quadrant appear yellow.[36,37] PP1-D63 and PP2-D63 differ significantly in optical birefringence, spherulite size and hence nucleus density. The spherulites of PP1-D63 are coarse compared to PP2-D63 which confirms the high degree of nucleation for PP2. Yet, PLM provides neither information about crystallinity nor the quantitative ratio of polymorphs. Therefore, sections over the pipe wall were analyzed by DSC (Figure 6).

PP1-D63 consists exclusively of the α-modification. Due to cooling conditions after the extrusion a slight variation in peak shape is observed over the pipe wall while the peak maximum

Table II. Spectral Characteristics of Parameters Determined by μFTIR

Parameter	IR mode[a]	Peak (cm^{-1})	Baseline (cm^{-1})	Integration limit (cm^{-1})
Crystallinity	CH_3 rock	998	1010–986	1010–998
	CH_2 wag			
	CH bend			
Orientation	CH_3 rock	974	986–962	974–962
	r_{c-c}[b]			

[a] IR modes were observed by Ref. 34.
[b] r_{c-c} axial C–C stretching.

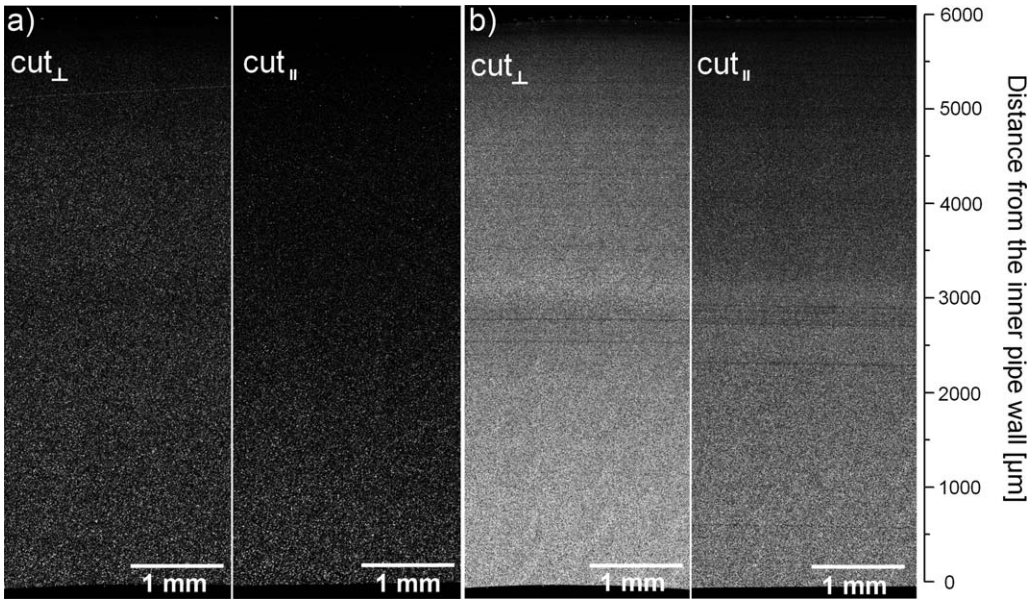

Figure 3. PLM images of cut $_{\perp}$ and cut $_{\parallel}$ cross-sections for (a) PP1-D63 and (b) PP2-D63.

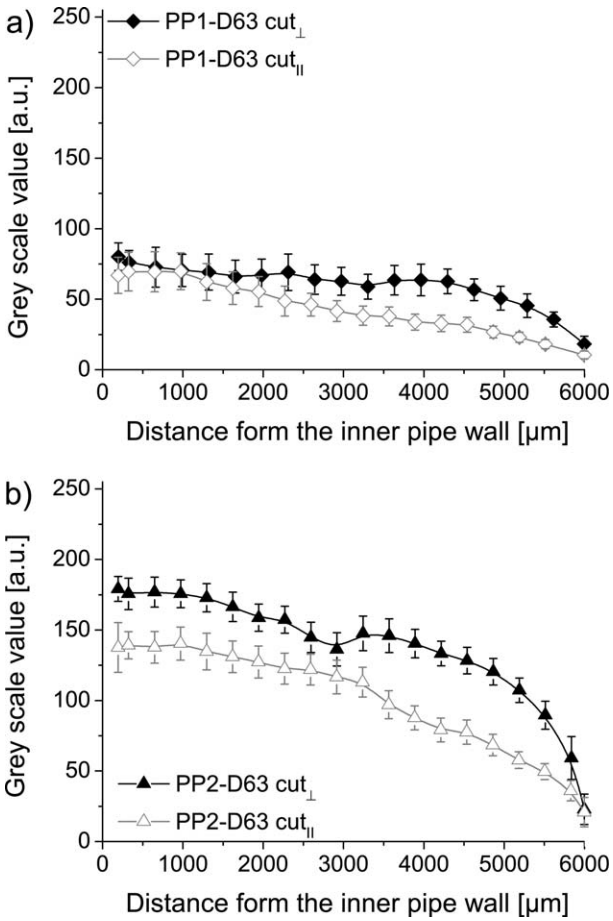

Figure 4. Histogram of (a) PP1-D63 and (b) PP2-D63 PLM images, see Figure 3.

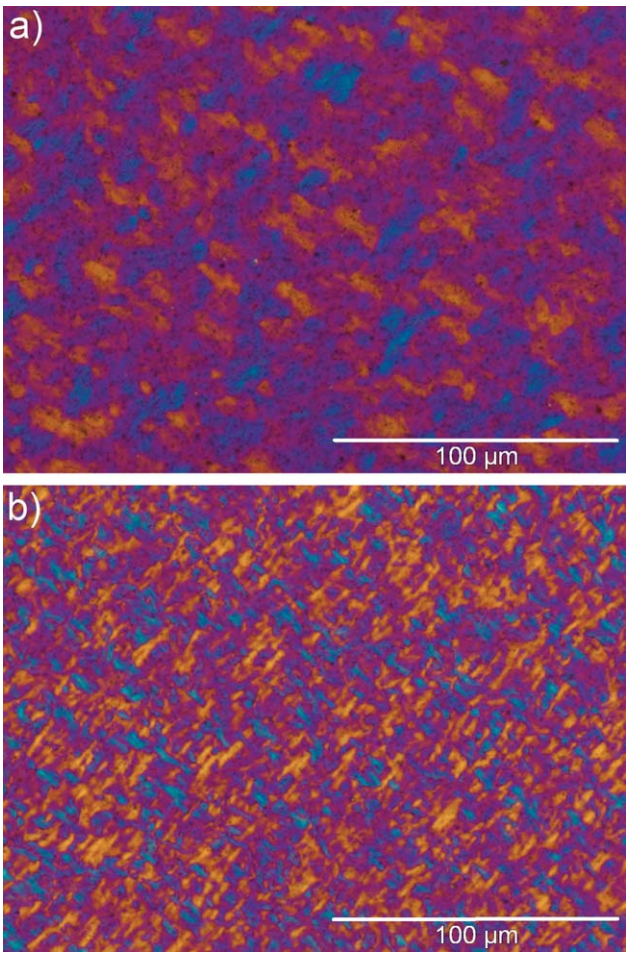

Figure 5. Magnification from the inner part of pipe (a) PP1-D63 cut $_{\perp}$ and (b) PP2-D63 cut $_{\perp}$. [Color figure can be viewed in the online issue, which is available at wileyonlinelibrary.com.]

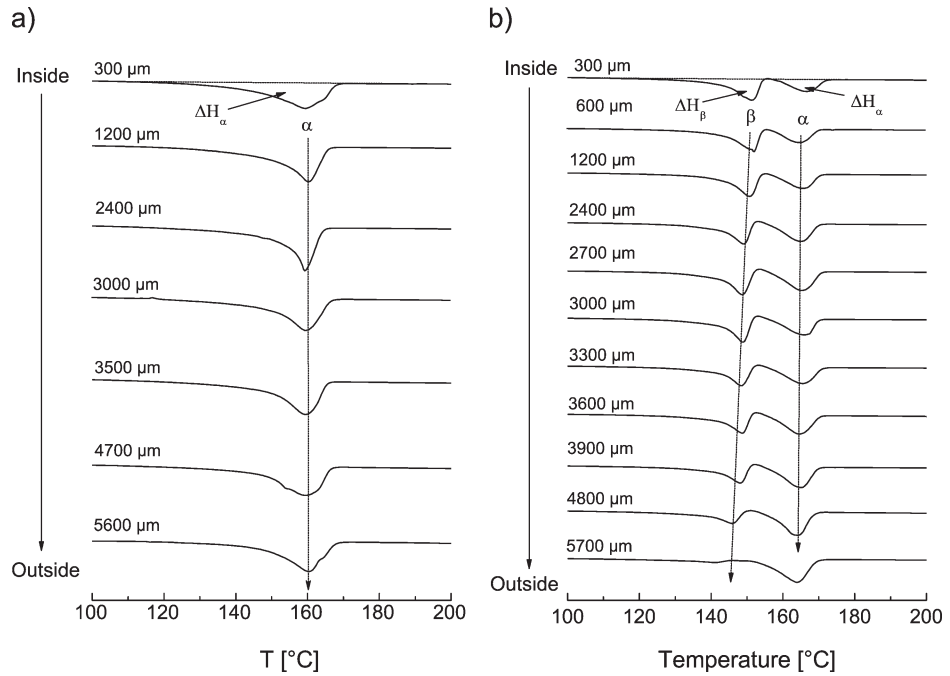

Figure 6. Melting endotherms (first heating) of microtomed samples taken over the pipe wall for (a) PP1-D63 and (b) PP2-D63. *Y*-Axis range is −2.0 to 0.25 W/g, respectively.

remains quite constant at around 160°C, except for the cut at the surface which shows a higher melting temperature. Because the melting temperature depends on the contact area in the DSC pan, this might be explained by the curved shape of the pipe surface. PP2-D63 shows two melting events at almost every position, with the first one at 150°C caused by the β-modification and the second one at around 165°C belonging to the α-modification.[38] Due to the cooling conditions after extrusion the quantity of the β-modification decreases to the outer surface of the wall and finally disappears. The degree of crystallinity, as well as the portion of β-modification, K_β, are tabulated in Table III and plotted as a function of their spatial coordinate in Figure 7.

Table III. X_C^{DSC} and K_β for PP1-D63 and PP2-D63

Distance from the inner pipe wall (µm)	PP1-D63	PP2-D63		
	X_C^{DSC} (%)	X_C^{DSC} (%)	K_β (%)	$\frac{K_\beta}{X_C^{DSC}}$ [a]
5700	48	47	24	0.51
4800	48	50	44	0.88
3900		50	50	0.99
3600	51	49	53	1.08
3300		54	59	1.09
3000	52	54	64	1.18
2700		59	60	1.02
2400	51	53	59	1.11
1200	53	53	66	1.24
600		51	68	1.35
300	51	51	68	1.32

[a] Extracted DSC parameter used in µFTIR section for comparison.

X_C^{DSC} coincides in the inner and outer region of the wall for both pipes, while significant differences are observed in the middle section where PP2-D63 shows a pronounced maximum which is missing for PP1-D63. The higher X_C^{DSC} for PP2-D63 might be explained by the higher efficiency of the respective nucleating agent.

The histogram from PLM (Figure 4) and the profile of X_C^{DSC} (Figure 7) are in good agreement for PP1-D63 except for the outer part of the wall. This difference might be explained by the drop of spherulite size in direction of the outer wall surface. Detailed magnification of the outer part of the pipe showed, that between 100 and 300 µm no spherulites are visible by PLM. However, for PP2-D63, dissimilarities between X_C^{DSC} and the PLM histogram are noticeable. These divergences might be

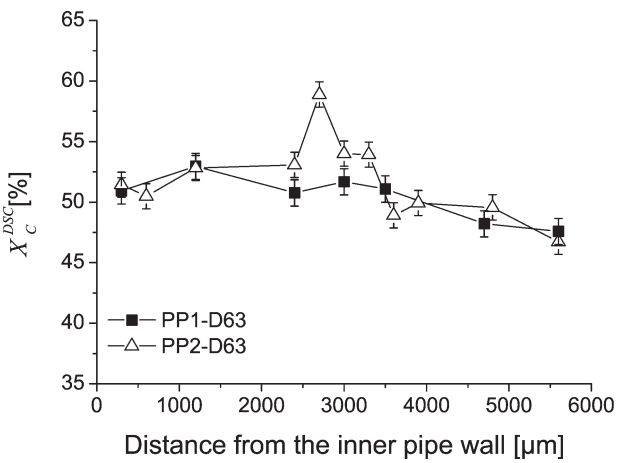

Figure 7. X_C^{DSC} profile over the pipe wall of PP1-D63 and PP2-D63.

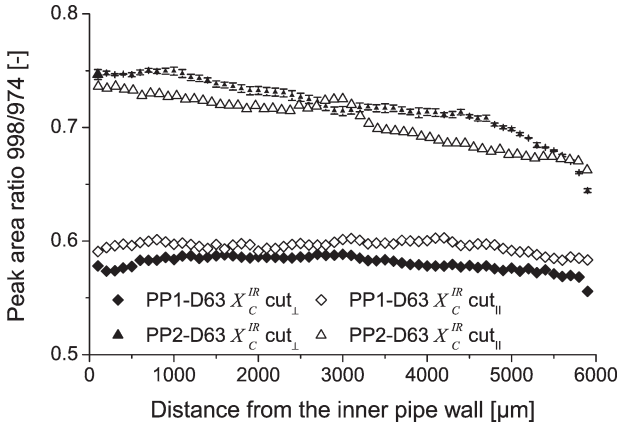

Figure 8. X_C^{IR} over the wall of the pipes and the average error for PP2-D63. Cut$_\perp$ and cut$_{||}$ were used, respectively.

explained by polymer chain orientation, which only influences PLM but not DSC.

µFTIR can also be used to profile the degree of crystallinity, X_C^{IR}, and in the case of PP the band at 998 cm^{-1} is caused by the crystalline portion,[39–41] whereas that at 974 cm^{-1} can be used as reference band.[42] Therefore, the band ratio 998/974 is frequently used for X_C^{IR} measurements.[28,39,43–45] Figure 8 shows the profiles of X_C^{IR}.

The profiles of cut$_\perp$ and cut$_{II}$ for X_C^{IR} differ slightly for both samples. PP1 shows an almost constant X_C^{IR} over the pipe wall for both cuts, whereas X_C^{IR} decreases monotonously from the inner toward the outer wall surface in the case of PP2. In Figure 9, the results of X_C^{DSC} and the X_C^{IR} profiles are compared. Because there is a difference in the X_C^{IR} profile of the two orthogonal microtome cuts, the two profiles are averaged.

For PP1-D63 the trends of X_C determined by µFTIR and DSC correlate well, but in the case of PP2-D63 clear differences become visible: At least the maximum of X_C^{DSC} in the center of the pipe wall is explainable because the cooling rate after extrusion is the lowest at that position. To identify a correlation Figure 10 compares the profiles of X_C^{IR} for the orthogonal cuts with that of X_C^{DSC} for PP2-D63.

The IR profiles for both cuts decrease from the inner to the outer wall, with cut$_{II}$ showing a maximum in the center. Taking into account that the range of X_C^{DSC} covered by both is comparable and that the scanned volume and thus the number of crystal units is equal for both cuts, the β nucleation must affect the band at 998 cm^{-1} in a different way. A closer look reveals that in both microtome cuts the band ratio 998/974 depends on K_β. Thus, the profile of X_C^{IR} of cut$_{II}$ was compared to that of K_β obtained by DSC. The results are illustrated in Figure 11.

It becomes evident that the two curves are in good agreement. Therefore, the band at 998 cm^{-1} of cut$_{II}$ is dominated by the β-modification. Because the band at 998 cm^{-1} of cut$_\perp$ shows a different profile, it seems that this band is affected by the nucleated β-modification in another way. Thus, the ratio of K_β

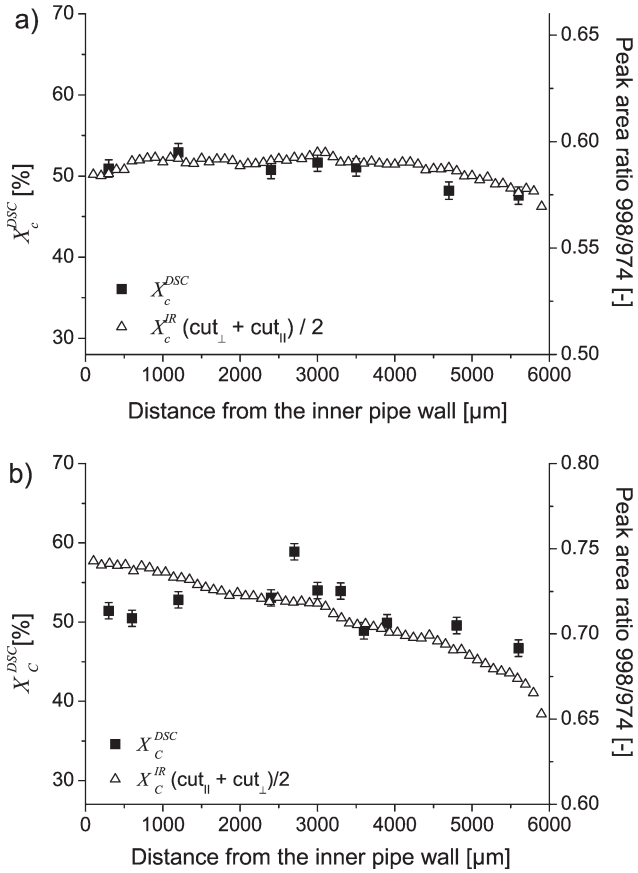

Figure 9. X_C of (a) PP1-D63 and (b) PP2-D63 measured by DSC and µFTIR.

and X_C^{DSC} was calculated and compared with the profile of X_C^{IR}. Figure 12 shows the correlation between K_β/X_C^{DSC} and the profile of 998 cm^{-1} for cut$_\perp$.

The two profiles are in respectable agreement and, therefore, the assumption was made that this profile is dominated by K_β and X_C^{DSC}. The additional dependence of X_C for cut$_\perp$ on the IR profile indicates an orientation-induced anisotropy of the crystalline part of the sample.

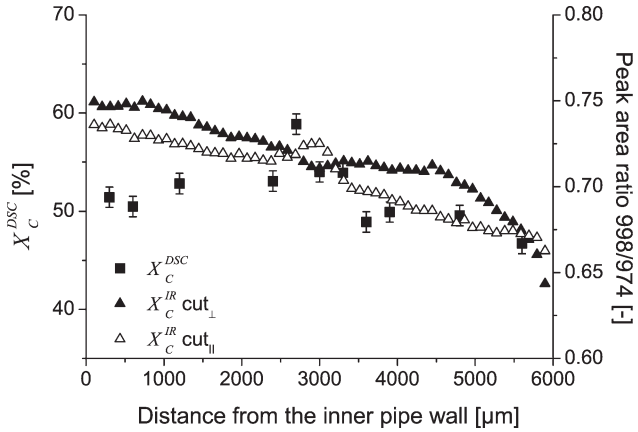

Figure 10. Profiles for X_C^{DSC} and X_C^{IR} of PP2-D63.

Applied Polymer SCIENCE

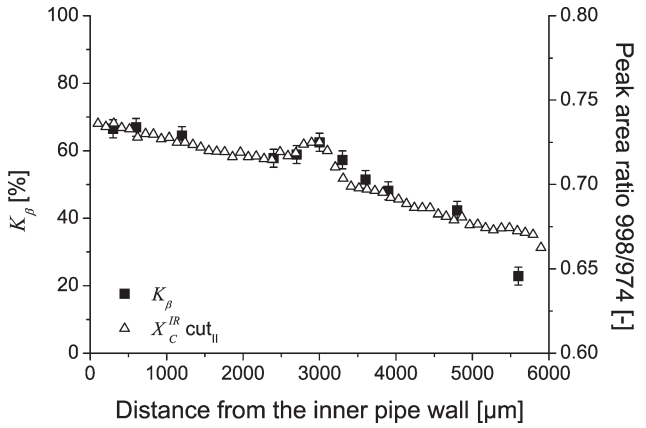

Figure 11. Profiles of K_β measured by DSC and X_C^{IR} for cut$_{II}$ of PP2-D63.

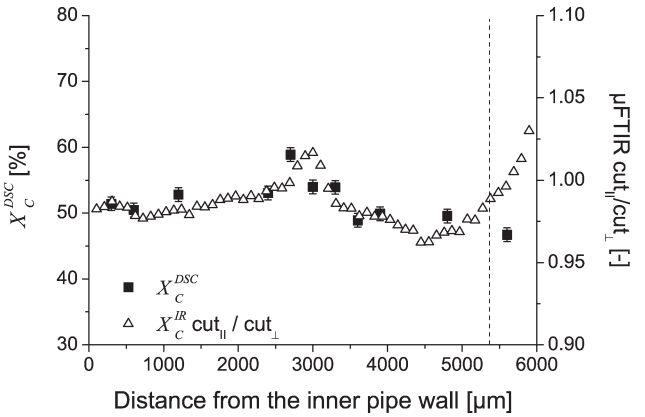

Figure 13. Profile of X_C^{DSC} and X_C^{IR} profile of cut$_{II}$/cut$_\perp$ for PP2-D63. The dashed line indicates outer layer of the pipe.

Empirically for samples containing the β-polymorph it could be determined that for cut$_\perp$ the peak area ratio 998/974 is proportional to K_β/X_C^{DSC}, and for cut$_{II}$ proportional to K_β. Considering the calculation limits, these relationships do not apply for very low crystallinity, because K_β/X_C^{DSC} runs in this case to infinity. Orthogonality of both microtome cuts is a prerequisite and an accurate cognition of the MD direction is required, which defines the cut direction parallel and perpendicular to MD.

If the assumption is valid that the intensity of the band at 998 cm^{-1} depends on K_β and X_C^{DSC}, the ratio of X_C^{IR} for cut$_{||}$ and cut$_\perp$ should represent X_C^{DSC} as well. The result is presented in Figure 13.

As assumed the two profiles are in perfect match, except for the outer layer of the pipe. Taking into account the mentioned limitations this can be explained by the low amount of β-modification present in this region (see Table III). Because there are almost no β spherulites in the outer layer, as confirmed by DSC, the evaluation by µFTIR is unsecure in this region.

The change in crystallinity can be determined from the peak area ratio 998/974 of the individual parallel and perpendicular cuts by:

$$X_C^{DSC} = \frac{K_\beta}{\left(\frac{K_\beta}{X_C^{DSC}}\right)} \sim \frac{\frac{A_{998}}{A_{974}}(\text{cut}_{II})}{\frac{A_{998}}{A_{974}}(\text{cut}_\perp)}$$

Additionally the histograms of PP2-D63 [see Figure 4(b)] are in remarkably good agreement with the results obtained by µFTIR (Figure 8). Therefore, in an analogue manner to the evaluation of X_C^{IR}, the ratio of the two profiles was calculated (Figure 14).

It can be noticed that the histogram quotient of cut$_{II}$/cut$_\perp$ matches the µFTIR profile (see Figure 13) as well. This unexpected shape of the profile indicates also a correlation to the results of X_C determined by DSC and µFTIR. Using these relationships µFTIR can be used to profile the degree of crystallinity in β-nucleated PP.

The fourth morphological parameter which has to be considered is the orientation of the polymer chains. As shown, anisotropy with regard to the latter influences the IR absorption used to calculate the degree of crystallinity. A method to determine the orientation of polymer chains in the three directions from the dichroism of IR-absorptions was recently derived on a theoretical basis by Rode et al. The method uses measurements of two perpendicular microtome cuts corresponding to the axes of

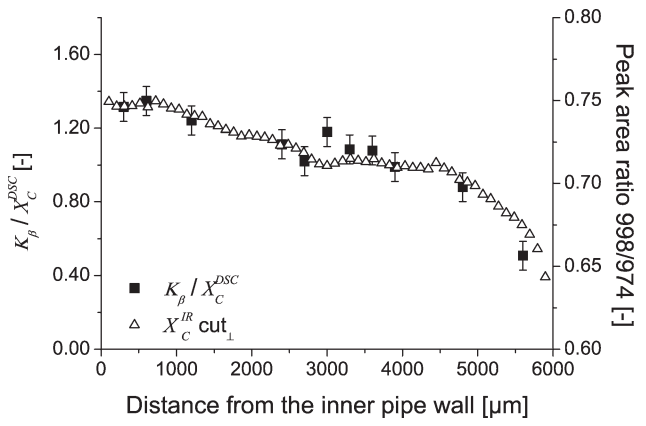

Figure 12. K_β/X_C^{DSC} as measured by DSC versus X_C^{IR} profile of cut$_\perp$ determined for PP2-D63.

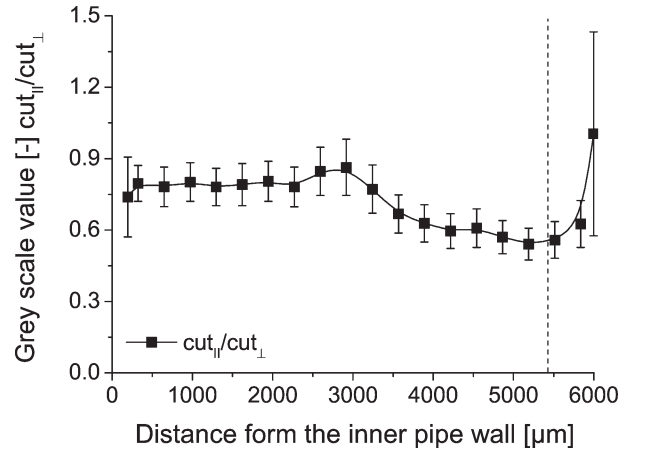

Figure 14. Histogram profile of PP2-D63 cut$_{||}$/cut$_\perp$. Dashed line indicates outer layer of the wall.

a defined coordinate system. The orientation in three directions is calculated from the individual absorbance.[46]

In the case of PP the absorption at 974 cm^{-1} is affected by both the amorphous and the crystalline phase.[47] To calculate an average orientation of the chain axis for both phases, the samples were measured as described in the experimental part using linear polarized IR-light. The profiles for the calculated orientation in all three directions are presented in Figure 15.

The MD-orientation of the polymer chains in PP1-D63 increases constantly from the inside to the outside of the wall, whereas for ND an opposite behavior is observed. This is caused by the shear field of the extrusion and the fact that solidification starts from both surfaces, i.e., the anisotropy incurred by the shear field of the extrusion is frozen, at a faster rate from the outer surface due to quenching. Both directions show a slight minimum in the middle of the wall, which is due to the fact that the polymer stays molten in this region for the longest time and thus the induced orientation can maximally relax. No orientation in TD is observed. For PP2-D63 the orientation in MD monotonously increases from the inner to the outer surface, with a steep increase in the last 500 µm. Similar to the PP1 sample this is the result of the shear field and cooling conditions. The orientation in TD and ND is V shape with a pronounced minimum at the center of the wall, where consequently the polymer chains have no preferential orientation in TD and ND. As discussed before, relaxation of the molecules and isotropic crystal growth are supported in the pipe center.

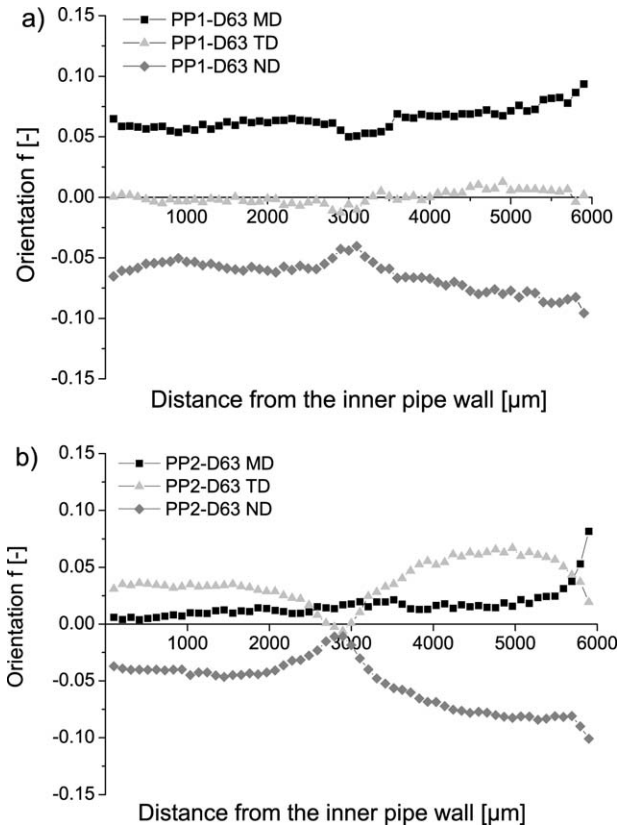

Figure 15. Orientation of (a) PP1-D63 and (b) PP2-D63 over the pipe wall in all three directions.

CONCLUSIONS

Depending on the conditions applied in the extrusion process, polymers are spatially distributed with regard to their morphological parameters, i.e., degree of crystallinity, polymorphism and chain orientation. In this study the molecular orientation and morphology of an α- and β-nucleated PP pipe were studied by DSC, µFTIR and PLM. For the α-nucleated specimen the degree of crystallinity can be derived from the specific IR-bands in a straightforward manner. However, in the case of β-nucleated PP this approach fails and the thus determined crystallinity profile depends on the direction of inspection, i.e., it is influenced by a preferential orientation incurred by the β-polymorph. This problem can be can be overcome by correlating the results of µFTIR with those from DSC. In detail, it could be shown that the area ratio of the IR-bands used to calculate the degree of crystallinity is proportionate to K_β/X_C^{DSC} for the perpendicular cut and proportionate to K_β for the parallel cut. Thus, it is now possible to exploit the advantages of µFTIR, i.e., high spatial resolution and speed of measurement, also for morphology profiling in the case of β-nucleated PP. For the first time, the previously theoretically derived model was experimentally applied to determine molecular orientation. It could be shown that the orientation profile of the polymer chains over the wall as determined from the IR-dichroism reflects the shear field during the extrusion, the post extrusion cooling history, and the specific nucleation. For pipes of both polymorphs, a higher degree of orientation is found at the outer wall surface where the quenching freezes the incurred molecular anisotropy. For both the samples, the orientation passes a minimum at the center of the wall.

ACKNOWLEDGMENTS

The financial support by the "Bundesministerium für Wirtschaft und Technologie" (BMWi) through "Arbeitsgemeinschaft industrieller Forschungsvereinigungen e.V." (AiF) is gratefully acknowledged (IGF Research Project no. 15 806 N). In particular, we thank Dr. Heinz Vogt (Basell Polyolefine GmbH) for fruitful discussions.

REFERENCES

1. Dragaun, H. *Prog. Colloid Polym. Sci.* **1977**, *62*, 59.
2. Varga, J.; Schulek-Tóth, F. *J. Therm. Anal. Calorim.* **1996**, *47*, 941.
3. Varga, J.; Mudra, I.; Ehrenstein, G. W. *J. Appl. Polym. Sci.* **1999**, *74*, 2357.
4. Juhász, P.; Varga, J.; Belina, K.; Belina, G. *J. Macromol. Sci. Part B* **2002**, *41*, 1173.
5. Menyhárd, A.; Varga, J.; Molnár, G. *J. Therm. Anal. Calorim.* **2006**, *83*, 625.
6. Libster, D.; Aserin, A.; Garti, N. *Polym. Adv. Technol.* **2007**, *18*, 685.
7. Tjong, S. C.; Xu, S. A. *Polym. Int.* **1997**, *44*, 95.

8. Mubarak, Y.; Martin, P. J.; Harkin-Jones, E. *Plast. Rubber Compos.* **2000**, *29*, 307.
9. Wang, K.; Mai, K.; Han, Z.; Zeng, H. *J. Appl. Polym. Sci.* **2001**, *81*, 78.
10. Marco, C.; Gómez, M. A.; Ellis, G.; Arribas, J. M. *J. Appl. Polym. Sci.* **2002**, *86*, 531.
11. Marco, C.; Ellis, G.; Gómez, M.; Arribas, J. *J. Therm. Anal. Calorim.* **2002**, *68*, 61.
12. Leugering, V. H. *J. Die Makromol. Chem.* **1967**, *109*, 204.
13. Keith, H. D.; Padden, F. J.; Walter, N. M.; Wyckoff, H. W. *J. >Appl. Phys.* **1959**, *30*, 1485.
14. Padden, F. J.; Keith, H. D. *J. Appl. Phys.* **1959**, *30*, 1479.
15. Jones, A. T.; Aizlewood, J. M.; Beckett, D. R. *Die Makromol. Chem.* **1964**, *75*, 134.
16. Fitchmun, D. R.; Mencik, Z. *J. Polym. Sci.: Polym. Phys. Ed.* **1973**, *11*, 951.
17. Fleischmann, E.; Zipper, P.; Jánosi, A.; Geymayer, W.; Koppelmann, J.; Schurz, J. *Polym. Eng. Sci.* **1989**, *29*, 835.
18. Varga, J. *J. Mater. Sci.* **1992**, *27*, 2557.
19. Ariyama, T. *J. Mater. Sci.* **1992**, *27*, 4940.
20. Fujiyama, M. *Int. Polym. Process.* **1995**, *10*, 172.
21. Fujiyama, M. *Int. Polym. Process.* **1995**, *10*, 251.
22. Dragaun, H.; Hubeney, H.; Muschik, H.; Detter, G. *Kunststoffe* **1975**, *65*, 311.
23. Geertz, G.; Brüll, R.; Wieser, J.; Maria, R.; Wenzel, M.; Engelsing, K.; Wüst, J.; Bastian, M.; Rudschuck, M. *Polym. Degrad. Stab.* **2009**, *94*, 1092.
24. Maria, R.; Rode, K.; Brüll, R.; Dorbath, F.; Baudrit, B.; Bastian, M.; Brendlé, E. *Polym. Degrad. Stab.* **2011**, *96*, 1901.
25. Hong, Z.; Cong, Y.; Qi, Z.; Li, H.; Zhou, W.; Chen, W.; Wang, X.; Zhou, Y.; Li, L. *Polymer* **2012**, *53*, 640.
26. Ellis, G.; MA, G.; Macro, C. *Internet J. Vib. Spectro.* **2001**, 5..
27. Wenzel, M.; Brüll, R.; Geertz, G.; Engelsing, K.; Wüst, J.; Bastian, M. *3R Int.* **2007**, *12*, 819.
28. Brüll, R.; Geertz, G.; Kothe, H.; Macko, T.; Rudschuck, M.; Wenzel, M.; Engelsing, K.; Wüst, J.; Bastian, M. *Macromol. Mater. Eng.* **2008**, *293*, 400.
29. Shi, G.-y.; Zhang, X.-d.; Qiu, Z.-x. *Die Makromol. Chem.* **1992**, *193*, 583.
30. Gahleitner, M.; Wolfschwenger, J.; Bachner, C.; Bernreitner, K.; Neißl, W. *J. Appl. Polym. Sci.* **1996**, *61*, 649.
31. Li, J. X.; Cheung, W. L.; Jia, D. *Polymer* **1999**, *40*, 1219.
32. Varga, J.; Stoll, K.; Menyhárd, A.; Horváth, Z. *J. Appl. Polym. Sci.* **2011**.
33. Houska, M.; Brummell, M. *Polym. Eng. Sci.* **1987**, *27*, 917.
34. Miyazawa, T.; Ideguchi, V.; Fukushima, K. *J. Chem. Phys.* **1963**, *38*, 2709.
35. Davidson, M. W. The First Order (Full Wave) Retardation Plate. http://olympusmicro.com/primer/techniques/polarized/firstorderplate.html.
36. Sawyer, L. C.; Grubb, D. T.; Meyers, G. F. Polymer Microscopy; Springer: New York, **2008**; p 1.
37. Suefusa, K.; Monobe, K. The Optical Behavior of Polyethylene Spherulites; Memoirs of the School Of Engineering, Okayama University **1968**, *3*, 95.
38. Jacoby, P.; Bersted, B. H.; Kissel, W. J.; Smith, C. E. *J. Polym. Sci.: Part B: Polym. Phys.* **1986**, *24*, 461.
39. Luongo, J. P. *J. Appl. Polym. Sci.* **1960**, *3*, 302.
40. Painter, P. C.; Watzek, M.; Koenig, J. L. *Polymer* **1977**, *18*, 1169.
41. Tadokoro, H.; Kobayashi, M.; Ukita, M.; Yasufuku, K.; Murahashi, S.; Torii, T. *J. Chem. Phys.* **1965**, *42*, 1432.
42. Stein, R. S.; Finkelstein, R. S. *Annu. Rev. Phys. Chem.* **1973**, *24*, 207.
43. Quynn, R. G.; Riley, J. L.; Young, D. A.; Noether, H. D. *J. Appl. Polym. Sci.* **1959**, *2*, 166.
44. Ellis, G.; Marco, C.; Gómez, M. A.; Collar, E. P.; García-Martínez, J. M. *J. Macromol. Sci. Part B* **2005**, *43*, 253.
45. Karacan, I.; Benli, H. *J. Appl. Polym. Sci.* **2012**, *124*, 3037.
46. Brüll, R.; Maria, R.; Rode, K. *Macromol. Chem. Phys.* **2010**, *211*, 2233.
47. Bayer, G.; Hoffmann, W.; Siesler, H. W. *Polymer* **1980**, *21*, 235.